Hindawi Publishing Corporation
Journal of Nanomaterials
Volume 2016, Article ID 7617894, 10 pages
http://dx.doi.org/10.1155/2016/7617894

Research Article

Paramagnetic Gd_2O_3 Nanoparticle-Based Targeting Theranostic Agent for C6 Rat Glioma Cell

Seong-Pyo Hong,[1] Seong Hee Kang,[1] Do Kyung Kim,[2] and Bo Sun Kang[1]

[1]*Department of Radiological Science, Konyang University, Daejeon 302-718, Republic of Korea*
[2]*College of Medicine, Konyang University, Daejeon 302-718, Republic of Korea*

Correspondence should be addressed to Bo Sun Kang; bskang@konyang.ac.kr

Received 30 December 2015; Revised 9 March 2016; Accepted 3 April 2016

Academic Editor: Muhammet S. Toprak

This study aimed to synthesize theranostic agent targeting C6 rat glioma cell, which was based on the dextran coated paramagnetic gadolinium oxide nanoparticles (D-PGONs) conjugated with folic acid (FA) or paclitaxel (PTX). The D-PGONs were synthesized by the *in situ* coprecipitation method, and the average value of the size distribution was 2.9 nm. FTIR spectroscopy was fulfilled to confirm the conjugations of FA or PTX with D-PGONs. The bioprotective effects of dextran coating and chemotherapeutic effect of PTX in the C6 glioma cell were evaluated by the MTT assay. The differences in uptakes between the synthesized theranostic agents into C6 cells were observed by confocal laser scanning microscopy. In addition, the magnetic contrast enhancement with different concentration of the synthesized agent was compared by the T_1-weighted MRI imaging. It was experimentally shown that the synthesized theranostic agent targets C6 cells due to the ligand-receptor-mediated endocytosis and provides enhancement in MR contrast depending on the concentration due to the paramagnetic property of gadolinium nanoparticle. In addition, it was shown by the results of MTT assay that the synthesized nanocomposites were more effective in reducing cell viability than bare gadolinium nanoparticles. In conclusion, it was shown that FA and PTX conjugated D-PGONs could be used as the theranostic agent with paramagnetism and chemotherapeutic property.

1. Introduction

Conventional diagnostic and therapeutic agents for cancer treatment such as contrast agent for MRI [1], drugs for chemotherapy [2], or radiolabeled biomolecules are often limited in applications by short blood circulation times, nonspecific biodistribution [3], and toxicity to normal organs. The limitations could be overcome by the nanotechnology by combining functionalities for therapy and diagnosis in a single nanocomposite [4, 5]. The term "theranostics" is a newly coined word to define ongoing efforts in clinics to develop more specific, individualized therapies for various diseases and to combine diagnostic and therapeutic capabilities into a single agent [6]. The researches on the nanoparticles for the theranostic agent have been accomplished in many research groups [7–9]. The development of theranostic agent is comprised of two phases in general. The first phase is synthesis of nanoparticles as the base matrix of the diagnostic agent; the second phase is the conjugation of various functional moieties on the surface of nanoparticles.

Magnetic resonance imaging (MRI) is one of the useful medical diagnosis modalities using magnetic resonance signals from a human [10]. Magnetic contrast agents are generally used in MRI to enhance the contrast between malignant lesions and normal tissues in a diagnostic image. An MRI contrast agent is mainly comprised of paramagnetic materials. Among the paramagnetic materials, gadolinium (Gd^{3+}) is the most commonly used rare-earth metal element for the positive contrast agent for MRI. Gd^{3+} is used in varied forms of chelated chemical complex because a free gadolinium ion shows high toxicity [11]. Hence the nanoparticles based on Gd^{3+} are also paramagnetic; gadolinium nanoparticles can be used for MRI contrast agent if they were synthesized in the optimized size and with stability in a biochemical system. Paramagnetic gadolinium oxide or

gadolinium hydroxide nanoparticles have been extensively studied with various ways of surface treatments and the functionalizations for MRI contrast agent [12, 13].

The surface treatment of nanoparticles with polymer is necessary to increase colloidal stability of the nanoparticles in the biochemical system and is essential for the functionalization of the nanoparticles by the chemical conjugation with functional moieties [14–21]. For example, dextran is one of the well-known polysaccharides for the surface treatment of nanoparticles for various purposes in the biomedical applications. Folic acid (FA) is a kind of vitamin and has also been used as a targeting molecule for folate receptor expressed cancers cell [22, 23]. Since the folate receptor is overexpressed on the membrane of certain cancer cells, the uptake of FA-conjugated nanoparticles into the cancer cell is efficiently increased by the receptor-mediated endocytosis [24, 25]. Besides, the C6 cell can be targeted by nanoparticles conjugated with FA because the folate receptors were overexpressed on cell [26]. Paclitaxel (PTX) is a promising effective anticancer agent against various human cancers [27]. However, there are difficulties for PTX to be used as an anticancer drug because of the nonselective cytotoxicity and poor solubility in water. Recently, a number of research groups have conducted experiments on the problems, and some reported that the selectivity and solubility in water were increased when PTX has been used in the form of nanocomposites conjugated with water-soluble polymer or viral vectors [19, 28, 29].

Glioblastoma multiforme (GBM) is the most common and aggressive malignant brain tumor in the central nervous system (CNS) [30–32]. The most widely used GBM cell lines in neurobiological research are C6 cell line cloned from a chemically induced rat GBM and immortalized glial cells of rat brain which is both astrocytic and oligodendrocytic [33–35].

We synthesized gadolinium base theranostic agent (FA-PTX-D-PGONs) which has both targeting functionality and chemotherapeutic functionality given by the conjugation with FA and PTX, respectively. The characteristic properties of synthesized nanocomposites were measured by the analysis on morphology, conjugated molecular structure, and magnetic contrast using TEM, FTIR, and MRI, respectively. Cytotoxicity and cellular uptake at C6 rat glioma cell *in vitro* were also analyzed by MTT assay and confocal scanning laser microscopy.

2. Experiment Details

2.1. Materials. All the chemicals and reagents were used in "as-is" form provided from the supplier without purification. Gadolinium chloride ($GdCl_3$, 99%) was purchased from Strem Chemicals, Inc. (Newburyport, USA). Dextran-10 (MW 10000) and N-hydroxysulfosuccinimide (sulfo-NHS) were purchased from Biosesang, Inc. (Korea). Paclitaxel was purchased from Samyang Genex Corporation (Korea), and 1,1′-carbonyldiimidazole (CDI) was purchased from Acros Organics (part of Thermo Fisher Scientific Co., Inc.) (Geel, Belgium). Epichlorohydrin (ECH), chloroacetic acid (CA), and folic acid (FA) were purchased from Daejung Chemicals & Metals Co., Ltd. (Korea). Ammonia solution (28~30%) and ethylenediamine (EDA) were purchased from Samchun Chemical Co., Ltd. (Korea). Dimethyl sulfoxide (DMSO), sodium hydroxide (NaOH), 1-ethyl-3-(3-dimethylaminopropyl) carbodiimide hydrochloride (EDC·HCl), 3-[4,5-dimethylthiazol-2-yl]-2,5-diphenyltetrazolium bromide (MTT), and fluorescein isothiocyanate (FITC) were purchased from Sigma-Aldrich. C6 cells (a rat glioma cell line) were purchased from the Korean Cell Line Bank (Korea). The 4′,6-diamidino-2-phenylindole- (DAPI-) conjugated mounting medium was purchased from Invitrogen (Karlsruhe, Germany). Enzyme-linked immunosorbent assay (ELISA) kits were bought from DRG Diagnostics (Marburg, Germany). Cyclodextrin was purchased from Junsei Co., Ltd. Dulbecco's modified eagle's medium (DMEM), penicillin/Strep amphotericin b, and fetal bovine serum (FBS) were purchased from Lonza.

2.2. Synthesis of Dextran Coated Gadolinium Oxide Nanoparticles (D-PGONs). Gadolinium chloride (0.66 g) was dissolved in double distilled water (ddH_2O, 25 mL) for the preparation of Gd^{3+} stock solution of the D-PGON synthesis. Gd^{3+} stock solution (6 mL) was added to ddH_2O (20 mL) in company with dextran-10 (0.5 g). When the added dextran was perfectly dissolved in the solution, the temperature of the solution was reduced to 4°C. A small amount of ice cooled ammonia solution was added dropwise to the solution with stirring until the pH range was 8–10. The mixture was stirred for 10 min at room temperature and then the mixture was kept stirring for an additional 1 hour at the raised temperature of 70°C to continue the synthetic reaction. Finally, the purified suspension of D-PGONs was obtained by the dialysis against ddH_2O (5 L, 7 hours × 3 times) with a dialysis membrane (cutoff molecular weight of 14,000 Da).

2.3. Dextran Shell Modifications: Crosslinking, Carboxymethylation, and Amine Group Activation (Amino-D-PGONs)

2.3.1. Crosslink of the Coated Dextran Shell. The purified suspension (20 mL) and epichlorohydrin (ECH, 5 mL) were poured into NaOH stock solution (25 mL of 2.5 M) and then the mixture was incubated for 24 hours at room temperature with continuous shaking to promote the interaction between aqueous and organic (ECH) phase. When the reaction was completed, the purified suspension of crosslinked dextran coated PGONs (CLD-PGONs) could be obtained by the dialysis against ddH_2O (5 L, 7 hours × 3).

2.3.2. Carboxymethylation. CLD-PGONs dispersed suspension (10 mL) was mixed to NaOH stock solution (10 mL, 0.1 M), and the mixture was incubated for 1 hour at room temperature. Chloroacetic acid (0.443 g) solution was added to the CLD-PGONs dispersed suspension (10 mL), and the mixture was heated up to 60°C in a water bath for 2 hours. Figure 1(a) shows the reaction of carboxymethylation. The purified suspension of carboxymethylated CLD-PGONs (CMD-PGONs) was obtained by the dialysis against ddH_2O (5 L, 7 hours × 3).

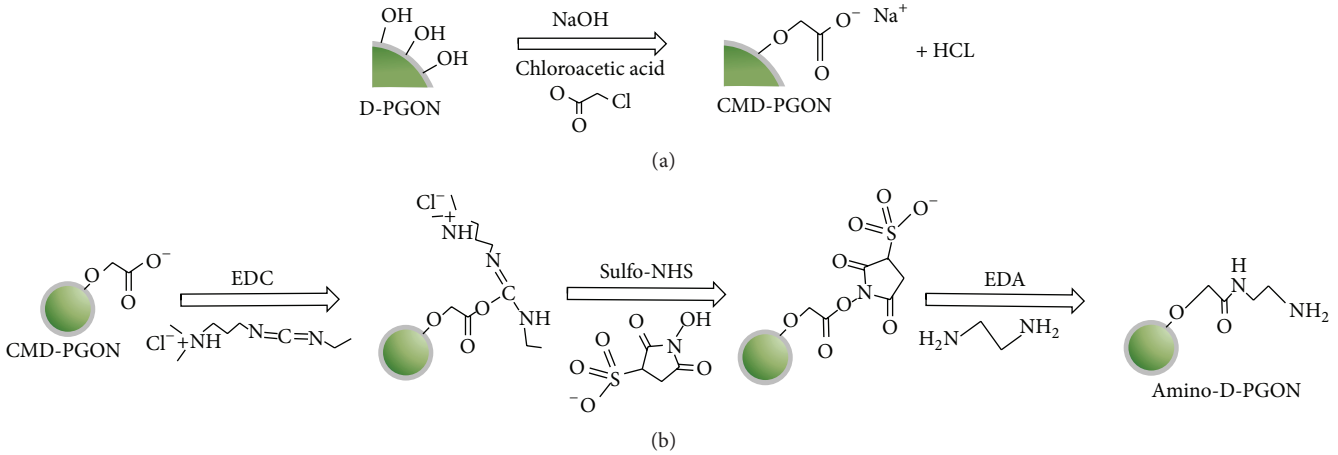

Figure 1: A synthetic scheme of (a) carboxymethyl group activation and (b) amine group activation.

2.3.3. Amine Group Activation. To activate carboxymethyl group of the CMD-PGONs, EDC·HCl (0.1 g) and sulfo-NHS (0.06 g) were added to CMD-PGONs dispersed suspension (10 mL), and the mixture was incubated for 15 min at RT. Ethylenediamine (3.5 mL) was added into the mixture for the activation of amine group and then the reaction mixture was incubated for a week at room temperature. The reaction is summarized in Figure 1(b). The purified suspensions of amine group activated CMD-PGONs (amino-D-PGONs) were obtained by the dialysis against ddH_2O, and finally the powder form of amino-D-PGONs could be obtained by vacuum drying of the suspension.

2.4. PTX Conjugation with Amino-D-PGONs (PTX-D-PGONs). Certain amount of PTX (2.8 mg) solution in DMSO (1 mL) was mixed with CDI (2.5 mg) dissolved in 1 mL DMSO (1 mL), and the activation of the hydroxyl group of PTX was continued at 50°C for 15 min. After the activation of hydroxyl group of PTX, amino-D-PGONs (10 mg) solution in DMSO (3 mL) was added to the activated PTX solution, and the reaction for the synthesis of PTX-D-PGONs was continued for 20 hours at 50°C. The reaction is summarized in Figure 2. PTX-D-PGONs dispersed suspension was purified by dialysis against both DMSO (50 mL, 10 hours × 2) and ddH_2O (5 L, 5 hours × 3). Finally, the powder form of the PTX-D-PGONs was obtained by vacuum drying of the suspension.

2.5. Preparation of FITC Labeled FA-Conjugated D-PGONs (FA-D-PGONs)

2.5.1. Folic Acid Conjugation with D-PGONs. To activate carboxyl groups of FA, a solution of FA (2.5 mg) and sulfo-NHS (3.8 mg) in DMSO (2 mL) was mixed with EDC·HCl (1.8 mg) solution in DMSO (2 mL), and the mixture was left for 5 min at 50°C. Subsequently, amino-D-PGONs (2.5 mg) solution in DMSO (1 mL) was added to the mixture, and the solution was left for 3 more hours again. The reaction is provided in Figure 3(a). When the conjugation was completed, the purified FA-D-PGONs suspension was obtained by dialysis against DMSO (50 mL, 7 hours × 2 times).

2.5.2. FITC Labeling on FA-D-PGONs. FITC stock solution (1 mg/mL) was prepared by resolving FITC (1 mg) in DMSO (1 mL). 100 μL of FITC stock solution was added to the purified FA-D-PGONs suspension and was stored at 50°C for 2 hours in the dark to synthesize FITC labeled FA-D-PGONs (FITC-FA-D-PGONs). Purified FITC-FA-D-PGONs suspension was obtained by dialysis against both DMSO (50 mL, 24 hours) and ddH_2O (5 L, 5 hours × 3).

2.6. Preparation of FA-PTX-D-PGONs. To activate carboxyl groups of FA, FA (1 mg) and sulfo-NHS (1.5 mg) solution in DMSO (2 mL) was mixed with EDC·HCl (0.7 mg) solution in DMSO (1 mL), and the mixture was left for 5 min at 50°C. Subsequently, PTX-D-PGONs (2.5 mg) solution in DMSO (3 mL) was added to the mixture, and the suspension was stored for 3 more hours. The reaction was summarized in Figure 3(b). At last, purified PTX-FA-D-PGONs suspension was obtained by dialysis against both DMSO (50 mL, 24 hours) and ddH_2O (5 L, 7 hours × 3).

2.7. Characterization. The morphology and nanostructure of the D-PGON were characterized by high-resolution transmission electron microscope (HR-TEM) JEM-2010 supplied by JEOL. Size distribution of synthesized nanocomposite was determined by Zetasizer Nano-S90 bought from Malvern. The molecular structure of synthesized nanocomposites was detected by the spectrum GX Fourier transform infrared (FTIR) spectroscopy of the Perkin Elmer with a wavenumber range of 4000–400 cm^{-1}. The magnetic property of the synthesized nanocomposites was measured by comparing pixel values of the MR images of the dilutions of the nanocomposite suspension with the different concentrations. The concentrations of the dilutions were 0, 86, 166, 249, 332, 415, and 489 μg/mL, respectively. The T_1 measurements were performed on the dilutions with a small animal 7 T MRI instrument (Bruker PharmaScan® MRI scanner, Germany). The averaged grayscale pixel values of each MR image were

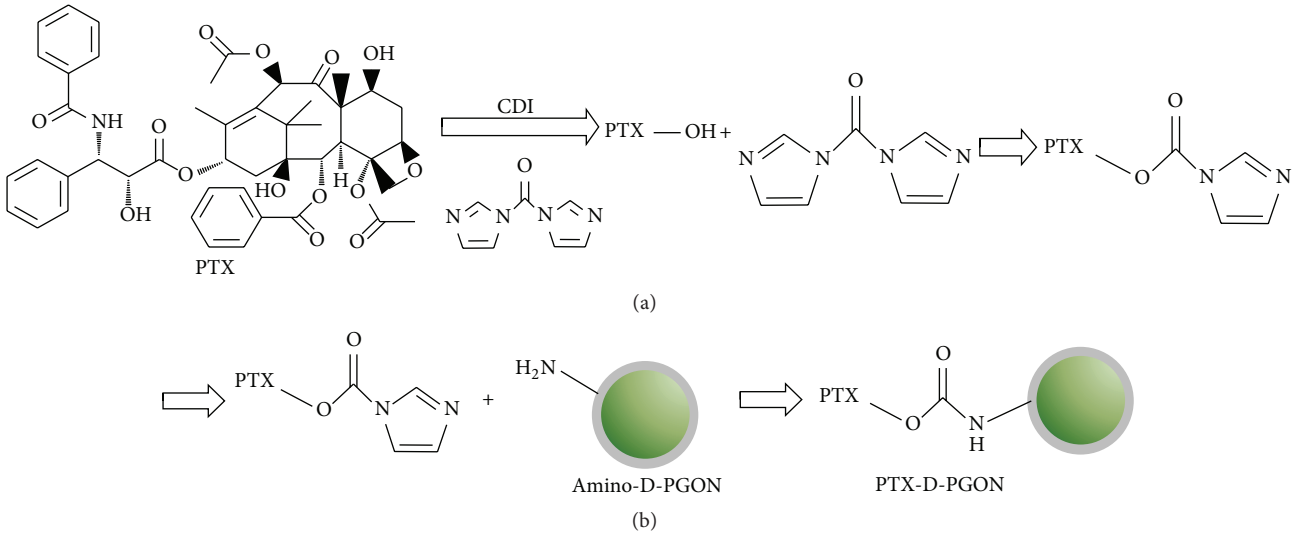

Figure 2: A synthetic scheme of (a) hydroxyl group activated PTX by using CDI and (b) PTX-D-PGON.

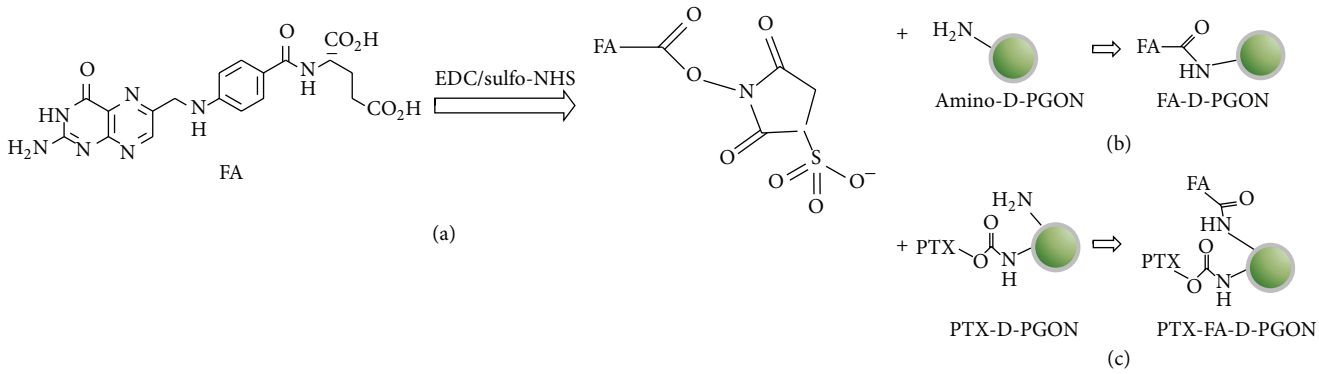

Figure 3: A synthetic scheme of (a) carboxyl group activated FA by using EDC/sulfo-NHS reaction, (b) FA-D-PGON, and (c) PTX-FA-D-PGON.

obtained by using "imageJ." The resultant measured values of each sample with different FA-PTX-D-PGONs concentrations (μg/mL) were plotted in Figure 8.

2.8. Cell Culture. C6 cells, rat glioblastoma cell line (Korean Cell Line Bank, Seoul, Korea) were cultured in Dulbecco's modified eagle's medium (DMEM) supplemented with 10% heat-inactivated fetal bovine serum (FBS) and 1% penicillin/streptomycin at 37°C in a humidified atmosphere of 5% CO_2. The cells were seeded at an initial density of 5×10^5 cells/mL in 75 cm^2 flask and passaged every third day.

2.9. Cell Viability. Cell viability at different concentration of nanocomposites was determined by the MTT assay. C6 cells were seeded in a 96-well plate at a density of 1×10^4 cells/100 μL and treated with different concentrations (10, 20, 40, 60, 80, 100, 300, and 500 μg/mL) of bare PGONs, CLD-PGONs, and FA-PTX-D-PGONs. The cells were kept in the culture medium for 24 hours. The cells were then incubated for 4 hours at 37°C with MTT (0.5 mg/mL, Sigma-Aldrich). The formazan crystals were generated by viable mitochondrial succinate dehydrogenase from MTT extracted using an equal volume of the solubilizing buffer (0.01 N HCl and 10% SDS). Absorbance of the MTT sample was measured at 540 nm wavelength in an ELx800UV microplate reader (BioTek Instruments, Inc.). The resultant data were expressed as the percentage of viable cells relative to untreated controls.

2.10. Internalization. The internalization of FA-PTX-D-PGONs in C6 cells was observed by confocal laser scanning microscopy (CLSM) (LSM5, Zeiss, Inc.). For the preparation of samples in microscopic observations, the C6 cells were seeded on cover glass in 12-well culture plates (5×10^4/well) and were incubated for 6 hours at 37°C in 5% CO_2 with FITC, FITC-D-PGONs, and FA-FITC-D-PGONs, respectively. The control cells were normally incubated at the same condition. After the incubation with nanocomposites, the samples were washed three times with PBS and fixed for 10 min at room temperature in PBS with 2% formaldehyde and 2% glutaraldehyde (1 : 1). Each sample was washed again and mounted on glass slide with mounting medium containing DAPI for 10 min at room temperature. Observations were

recorded with magnifier digital color camera (Optronics International, MA, USA). The fluorescence images were obtained at different excitation wavelengths for different fluorescent dyes, that is, at 405 nm for DAPI and 495 nm for FITC, respectively.

3. Results and Discussion

3.1. Dextran Coated Gadolinium Oxide Nanoparticles (D-PGONs). Paramagnetic gadolinium oxide nanoparticles with dextran coating on the surface (D-PGONs) were successfully synthesized by using *in situ* coprecipitation method. The method we used in this study is similar to the method reported by McDonald and Watkin, but the resultant nanocomposites of both methods were quite different in morphology and size [16]. Synthesis of ultrasmall size of gadolinium oxide nanoparticles with different protocols was previously reported by other research groups [12, 13, 36, 37]. The transparent colloid of gadolinium oxide nanoparticles was also synthesized by other research groups using different methods such as modified polyol method or modified thermal decomposition method [36]. Synthesized D-PGONs was transparent colloid and dispersed in water with high stability. Morphology of the D-PGONs is shown in Figure 4(a). The HR-TEM image confirms that the D-PGONs are of uniform ultrasmall size with diameters of sub 5 nm on average. Dynamic light scattering spectroscopy (DLS, Zetasizer) was utilized to evaluate the size distribution of D-PGONs. The average size was between 2~4 nm, and the histogram of measured size was shown in Figure 4(b).

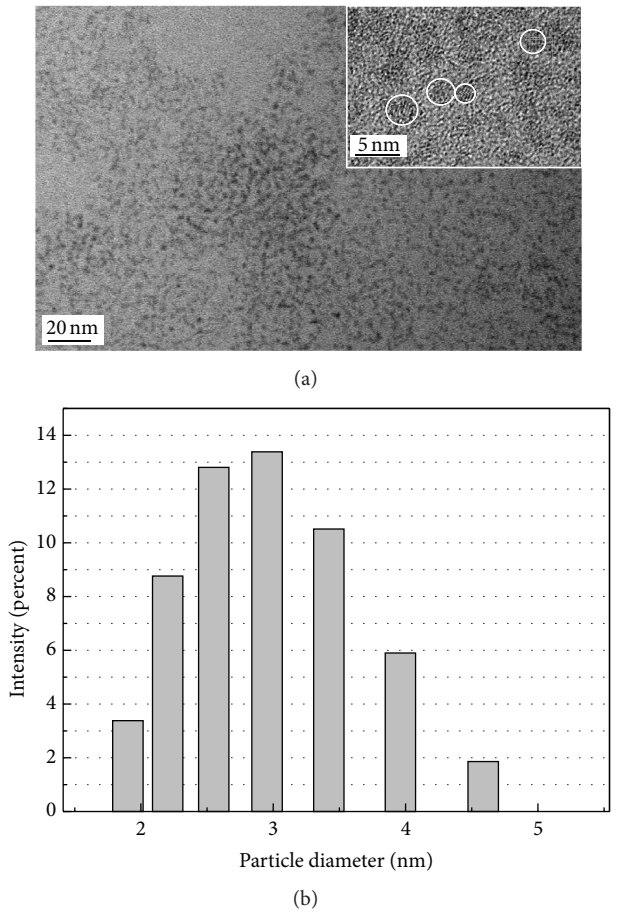

Figure 4: (a) TEM images of D-PGONs. (b) Particle size distributions of the D-PGONs, as measured by dynamic light scattering (DLS).

3.2. Characterization of Functionalized D-PGONs. Dextran coating is a weakly bonded shell that consisted of noncovalent binding of dextran molecules [15]. Bare gadolinium oxide nanoparticle (PGON) is needed to be completely isolated in the dextran shell during the usage because gadolinium is cytotoxic when it is released from the nanoparticle and exists as a free ion. Hence the crosslinking process on the dextran shell was applied using epichlorohydrin [14]. In general, dextran crosslinking process is applied before the conjugation of functional compounds to prevent the dextran shell dissociation.

The conjugation efficacy of PTX and FA could be quantitatively measured by UV/Vis absorption spectrometry with 260 nm UV and 360 nm UV, respectively [19]. In this study, the quantitative measurement of conjugation efficacy was not accomplished. Instead of it, the existence of FA and PTX in the synthesized nanocomposite (FA-PTX-D-PGONs) was confirmed by Fourier transform infrared (FTIR) spectroscopy. The conjugated functional groups (FA and PTX) could be characterized by comparison with the spectra of known chemical compound because the particular functional group is differentiated by the shape and relative intensities of the pulse in the specific region of the spectrum. Some of FTIR spectrums are exhibited as follows: the spectrum appears at 3580~3200 cm^{-1} that signifies the hydroxyl stretching in which the intensity of spectrum is lower and broader in proportion to the group's concentration increasing, primary amines spectrum is assigned in the region 3450~3250 cm^{-1} with a broadband and medium intensity, the region around 3000 cm^{-1} denotes aromatic C-H stretching, the carbonyl group is represented on the spectrum at 1850~1550 cm^{-1} due to C=O stretching vibration, the strong spectrum of 1260~100 cm^{-1} is assigned to C-O stretching, and the primary amines and secondary aliphatic amines occurred in the region 1090~1020 cm^{-1} with weak intensity and the region 1190~1170 cm^{-1} with medium intensity due to C-N stretching [38]. Through this database, pure paclitaxel and pure folic acid were characterized by a spectrum with characteristic peaks at 3339 (N-H stretching), 3319 (O-H stretching), 2973~2547 (aromatic C-H stretching vibrations), 1727, 1720 (C=O stretching vibrations), 1652~1579 (C-C ring stretching vibrations), 1274 (C-N vibrations), 1090, 1049 (C-O vibrations) cm^{-1} and 3543 (O-H stretching), 3416, 3324 (N-H stretching), 2959, 2924, 2844 (aromatic C-H stretching vibrations), 1694, 1640 (C=O stretching vibrations), 1605 (NH-vibration), 1484 (phenyl ring), and 1411 (OH deformation of phenyl skeleton) cm^{-1} [38, 39].

Measured FTIR spectra of the FA-PTX-D-SPGONs, pure FA, and pure PTX are shown in Figure 5. Some peaks shown in the FTIR spectrum of FA-PTX-D-SPIONs matched with

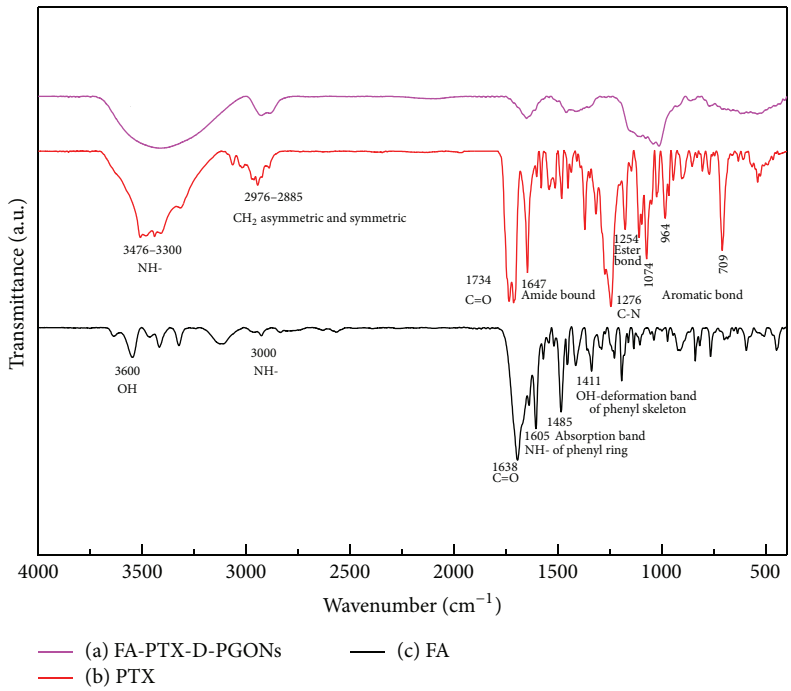

Figure 5: FTIR spectra of (a) FA-PTX-D-PGONs, (b) pure paclitaxel (PTX), and (c) pure folic acid (FA).

the peaks of pure PTX and pure FA [40]. In conclusion, PTX and FA are successfully conjugated with D-SPGONs.

3.3. Cytotoxicity. The bioprotective effect and chemotherapeutic effect of the FA-PTX-D-PGONs were evaluated by the MTT assay. We performed dose stability tests on C6 cells with different concentrations of bare PGONs, D-PGONs, and FA-PTX-D-PGONs as testing samples. The C6 cell viability of each sample was shown in Figure 6. The viability of C6 cells was inhibited by the synthesized nanocomposites in a dose-dependent manner. It was shown that the cell viability was over 90% regardless of the treated samples at the lower concentrations than 20 μg/mL, but the viability was decreased as the concentration increased. The viability decrement of the cell was larger in bare PGON treated group than the D-PGON group. The difference in viability seemed to be owing to the protective dextran shell on the D-PGON. In accordance with cell mortality, bare PGONs had more toxicity than D-PGONs in the C6 cells, and the crosslinked dextran shell had a bioprotective effect with 1.7% of cell mortality decrease. At the FA-PTX-D-PGONs treated group, the cell viability was significantly decreased as the concentration of FA-PTX-D-PGONs increased. The cytotoxicity of FA-PTX-D-PGONs is induced mainly by the PTX as it was reported by other research groups [41]. It is notable that the cytotoxicity of the bare PGON and D-PGON was increased with the increment of the concentrations of nanocomposites and saturated at the concentrations higher than 200 μg/mL. According to the diffusion equation, so-called Fick's law, the passive transportation $J(x)$ of the drug through the cell membrane is proportional to the gradient of the concentration across the membrane $\nabla n(x)$ with the diffusion coefficient D as shown below:

$$J(x) = -D \cdot \nabla n(x). \quad (1)$$

Therefore, the cellular uptake of the bare PGON and D-PGON is limited when the concentration of the medium and cytoplasm reaches equilibrium. In contrast, the cytotoxicity of the FA-PTX-D-PGONs was continuously decreased as the concentration increased much more than 200 μg/mL, because the active cellular uptake of the FA-PTX-D-PGONs was induced by the ligand-receptor-mediated endocytosis. It means that the FA-PTX-D-PGONs were selectively internalized by the folate receptors overexpressed at the membrane of cancer cells regardless of the concentration. Consequentially, it was confirmed that the FA-PTX-D-PGON was the effective drug delivery system for the cancer treatment, and it could be used for chemotherapeutic agent with the functionality of targeting cancer.

3.4. Folic Acid-Mediated Internalization. The intracellular uptake was compared between nanocomposites conjugated with FA and nonconjugated using confocal laser scanning microscopy (CLSM) to identify the efficacy of folic acid (FA) as a targeting molecule. For the CLSM analysis, fluorescein isothiocyanate (FITC) which is a commercially available fluorescent dye for CLSM was additionally conjugated to nanocomposites with or without FA. The CLSM images of C6 cells incubated with the FITC, FITC-D-PGONs, or FITC-FA-D-PGONs and the control were shown in Figure 7. The blue region of the image is the cell nuclei stained with DAPI (4′,6-diamidino-2-phenylindole), and the green region is the cytoplasm containing FITC conjugated nanocomposites

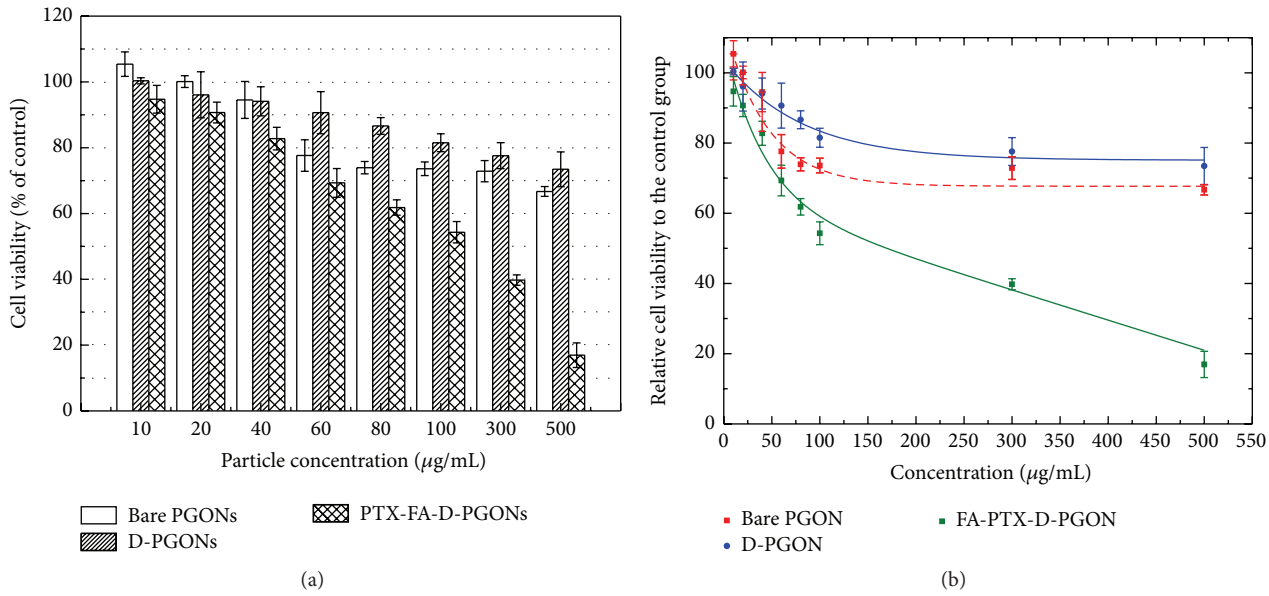

Figure 6: (a) Viability of C6 cell after 24 hrs of incubation with different concentration of bare PGONs, CLD-PGONs, and PTX-FA-D-PGONs. (b) Exponential fitting of C6 cell viability after 24 hrs of incubation with different concentration of bare PGONs, CLD-PGONs, and PTX-FA-D-PGONs.

which are delivered into by the folate receptor-mediated endocytosis. While the fluorescence emission of FITC was not observed in the control cells either the cells incubated with FITC diluted medium, it was observed in the cells incubated with FITC-D-PGONs or FITC-FA-D-PGONs. It means that the delivery of FITC into the cytoplasm was increased in amount or in rate when it was conjugated with nanoplatform. Besides, there was notable amount of difference in FITC fluorescence between cells incubated with FITC-D-PGONs or FITC-FA-D-PGONs as it is shown in Figures 7(c) and 7(d). The measured grayscale pixel values were 21.5 ± 2.6 and 64.2 ± 8.3 at the cell images incubated with FITC-D-PGONs or FITC-D-PGONs, respectively. Since the intensity of the fluorescence was linearly proportional to the amount of the fluorescent stain, the comparison of fluorescence intensities of CLSM images experimentally proved that the FA enhanced intracellular uptake of the nanocomposites when it was conjugated to the nanoplatform. The improvement in intracellular uptake by the conjugation of FA came from the increased endocytosis mediated by the ligand-receptor binding (FA and FA receptor binding) on the cell membrane. The results of CLSM analysis were consistent with other reports that the folic acid was suitable for targeting cancer which overexpresses folate receptor [39, 41]. Hence, these results demonstrated that the FA-PTX-D-SPGONs could be utilized for effective C6 cell targeting theranostic agent.

3.5. T_1-Weighted MRI Imaging. The FA-PTX-D-PGON was designed as a theranostic agent, including T_1-weighted positive MRI contrast agent and chemotherapeutic property for C6 cell. Cancer targeting and chemotherapeutical property were confirmed with experimental analysis as shown in prior results and discussions. The magnetic property as a T_1-weighted positive MRI contrast agent was measured by MR images of the FA-PTX-D-PGONs. Hence, T_1-weighted MR images with different concentrations in ddH_2O were obtained to assess the magnetic property of the FA-PTX-D-PGONs. Images were obtained by Bruker's PharmaScan® MRI scanner as shown in Figures 8(a)–8(g). The images show that the averaged pixel values are increased (brightened) with the increment in the concentration of FA-PTX-D-PGONs. It is caused by the magnetic property of Gd^{3+} ions in the samples. The averaged grayscale pixel values of the images were measured and plotted as a function of the concentration of the FA-PTX-D-PGONs as shown in Figure 8(h). According to the physics of magnetism, the MRI contrast has a linear dependence of the relative number density of magnetic atoms. The relative MR signal, R, of specific nuclear species relative to hydrogen atom in the gray matter is defined as shown below, where γ is the gyromagnetic ratio and n is the relative number density to a hydrogen atom and S is the spin quantum number [37, 42]:

$$R \equiv |\gamma|^3 \times n \times S(S+1). \quad (2)$$

Hence, the increment in the pixel value of MRI images with increased FA-PTX-D-PGONs concentration means that the FA-PTX-D-PGONs could enhance MRI contrast of the target organ into which they are delivered. It can be claimed based on the experimental results that the synthesized FA-PTX-D-PGONs could be used as the T_1-weighted MRI contrast agent.

4. Conclusion

FA-PTX-D-PGON was successfully synthesized for C6 glioma cell targeting theranostic agent, including T_1-weighted positive MRI contrast agent and chemotherapy.

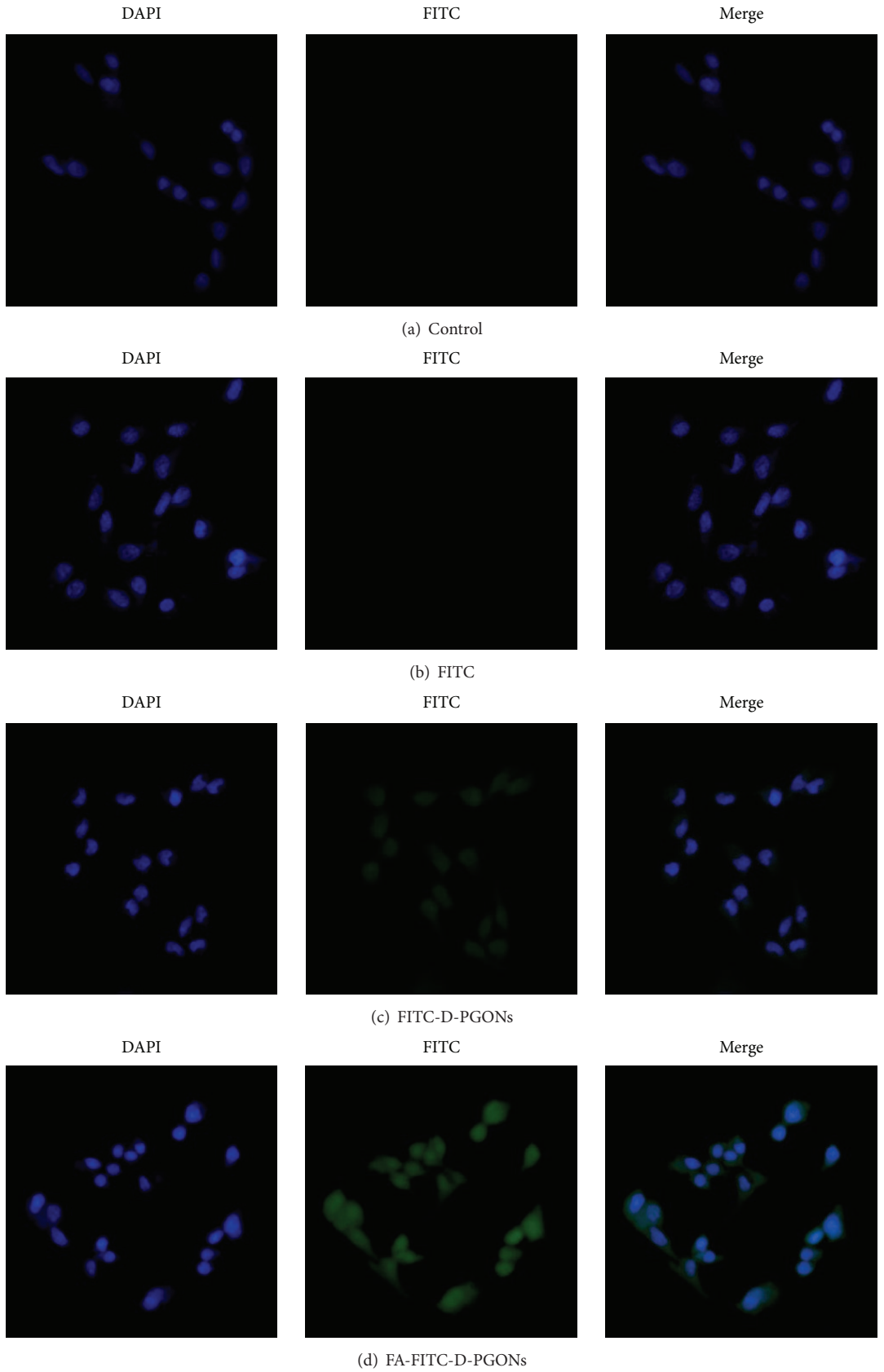

Figure 7: Confocal laser scanning microscopy of C6 cells which was incubated with different nanocomposites: (a) control, (b) FITC only, (c) FITC-D-PGONs, and (d) FA-FITC-D-PGONs. The three panels from left to right in each sample are the fluorescent images of DAPI, FITC, and merged image, respectively.

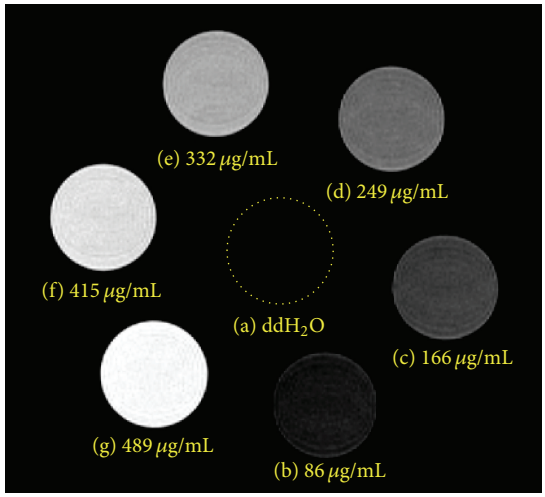

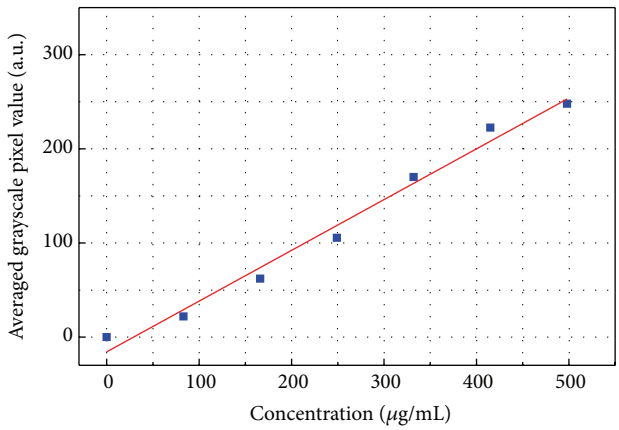

Equation	$y = a + b * x$
Weight	No weighting
Residual sum of squares	887.08214
Pearson's r	0.99218
Adj. R^2	0.98131

		Value	Standard error
Brightness	Intercept	−15.70786	9.0759
—	Slope	0.53914	0.03033

(h)

FIGURE 8: ((a)~(g)) T_1-weighted MRI images obtained from aqueous suspensions of PTX-FA-PGONs with different concentration. (h) Changes of MRI contrast as the function of PTX-FA-PGONs concentration.

The FA-PTX-D-PGON was evaluated by the MTT assay, confocal laser scanning microscopy, and MRI. It was shown that the FA-PTX-D-PGON was effectively delivered to the C6 cells by the FA to take advantage of the ligand-mediated endocytosis of the C6 cell.

Competing Interests

The authors declare that they have no competing interests.

References

[1] T. Grobner and F. C. Prischl, "Gadolinium and nephrogenic systemic fibrosis," *Kidney International*, vol. 72, no. 3, pp. 260–264, 2007.

[2] J. Wang, D. Short, N. J. Sebire et al., "Salvage chemotherapy of relapsed or high-risk gestational trophoblastic neoplasia (GTN) with paclitaxel/cisplatin alternating with paclitaxel/etoposide (TP/TE)," *Annals of Oncology*, vol. 19, no. 9, pp. 1578–1583, 2008.

[3] R. Bardhan, S. Lal, A. Joshi, and N. J. Halas, "Theranostic nanoshells: from probe design to imaging and treatment of cancer," *Accounts of Chemical Research*, vol. 44, no. 10, pp. 936–946, 2011.

[4] X. Wang, X. Sun, H. He et al., "A two-component active targeting theranostic agent based on graphene quantum dots," *Journal of Materials Chemistry B*, vol. 3, no. 17, pp. 3583–3590, 2015.

[5] M. K. Yu, J. Park, and S. Jon, "Targeting strategies for multifunctional nanoparticles in cancer imaging and therapy," *Theranostics*, vol. 2, no. 1, pp. 3–44, 2012.

[6] J. Xie, S. Lee, and X. Chen, "Nanoparticle-based theranostic agents," *Advanced Drug Delivery Reviews*, vol. 62, no. 11, pp. 1064–1079, 2010.

[7] K. Y. Choi, E. J. Jeon, H. Y. Yoon et al., "Theranostic nanoparticles based on PEGylated hyaluronic acid for the diagnosis, therapy and monitoring of colon cancer," *Biomaterials*, vol. 33, no. 26, pp. 6186–6193, 2012.

[8] J. E. Lee, N. Lee, T. Kim, J. Kim, and T. Hyeon, "Multifunctional mesoporous silica nanocomposite nanoparticles for theranostic applications," *Accounts of Chemical Research*, vol. 44, no. 10, pp. 893–902, 2011.

[9] D. Yoo, J.-H. Lee, T.-H. Shin, and J. Cheon, "Theranostic magnetic nanoparticles," *Accounts of Chemical Research*, vol. 44, no. 10, pp. 863–874, 2011.

[10] R. R. Edelman and S. Warach, "Magnetic resonance imaging," *The New England Journal of Medicine*, vol. 328, no. 10, pp. 708–716, 1993.

[11] P. Caravan, J. J. Ellison, T. J. McMurry, and R. B. Lauffer, "Gadolinium(III) chelates as MRI contrast agents: structure, dynamics, and applications," *Chemical Reviews*, vol. 99, no. 9, pp. 2293–2352, 1999.

[12] J. Y. Park, M. J. Baek, E. S. Choi et al., "Paramagnetic ultrasmall gadolinium oxide nanoparticles as advanced T_1 MRI contrast agent: account for large longitudinal relaxivity, optimal particle diameter, and in vivo T_1 MR images," *ACS Nano*, vol. 3, no. 11, pp. 3663–3669, 2009.

[13] Y.-S. Yoon, B.-L. Lee, K. S. Lee et al., "Surface modification of exfoliated layered gadolinium hydroxide for the development of multimodal contrast agents for MRI and fluorescence imaging," *Advanced Functional Materials*, vol. 19, no. 21, pp. 3375–3380, 2009.

[14] M. Lin, S. Li, H. H. Kim et al., "Complete separation of magnetic nanoparticles via chemical cleavage of dextran by ethylenediamine for intracellular uptake," *Journal of Materials Chemistry*, vol. 20, no. 3, pp. 444–447, 2010.

[15] C. Tassa, S. Y. Shaw, and R. Weissleder, "Dextran-coated iron oxide nanoparticles: a versatile platform for targeted molecular imaging, molecular diagnostics, and therapy," *Accounts of Chemical Research*, vol. 44, no. 10, pp. 842–852, 2011.

[16] M. A. McDonald and K. L. Watkin, "Investigations into the physicochemical properties of dextran small particulate

gadolinium oxide nanoparticles," *Academic Radiology*, vol. 13, no. 4, pp. 421–427, 2006.

[17] F. Dai, M. Du, Y. Liu, G. Liu, Q. Liu, and X. Zhang, "Folic acid-conjugated glucose and dextran coated iron oxide nanoparticles as MRI contrast agents for diagnosis and treatment response of rheumatoid arthritis," *Journal of Materials Chemistry B*, vol. 2, no. 16, pp. 2240–2247, 2014.

[18] K. Kumar, A. M. Nightingale, S. H. Krishnadasan et al., "Direct synthesis of dextran-coated superparamagnetic iron oxide nanoparticles in a capillary-based droplet reactor," *Journal of Materials Chemistry*, vol. 22, no. 11, pp. 4704–4708, 2012.

[19] J. Nakamura, N. Nakajima, K. Matsumura, and S.-H. Hyon, "Water-soluble taxol conjugates with dextran and targets tumor cells by folic acid immobilization," *Anticancer Research*, vol. 30, no. 3, pp. 903–909, 2010.

[20] P. Wunderbaldinger, L. Josephson, and R. Weissleder, "Crosslinked iron oxides (CLIO): a new platform for the development of targeted MR contrast agents," *Academic Radiology*, vol. 9, no. 2, pp. S304–S306, 2002.

[21] P. Caravan, "Protein-targeted gadolinium-based magnetic resonance imaging (MRI) contrast agents: design and mechanism of action," *Accounts of Chemical Research*, vol. 42, no. 7, pp. 851–862, 2009.

[22] Y. Lu, J. Wu, J. Wu et al., "Role of formulation composition in folate receptor-targeted liposomal doxorubicin delivery to acute myelogenous leukemia cells," *Molecular Pharmaceutics*, vol. 4, no. 5, pp. 707–712, 2007.

[23] Z. Zhang, S. Huey Lee, and S.-S. Feng, "Folate-decorated poly (lactide-co-glycolide)-vitamin E TPGS nanoparticles for targeted drug delivery," *Biomaterials*, vol. 28, no. 10, pp. 1889–1899, 2007.

[24] J. F. Ross, P. K. Chaudhuri, and M. Ratnam, "Differential regulation of folate receptor isoforms in normal and malignant tissues in vivo and in established cell lines: physiologic and clinical implications," *Cancer*, vol. 73, no. 9, pp. 2432–2443, 1994.

[25] C. Müller, A. Hohn, P. A. Schubiger, and R. Schibli, "Preclinical evaluation of novel organometallic 99mTc-folate and 99mTc-pteroate radiotracers for folate receptor-positive tumour targeting," *European Journal of Nuclear Medicine and Molecular Imaging*, vol. 33, no. 9, pp. 1007–1016, 2006.

[26] J. M. Saul, A. Annapragada, J. V. Natarajan, and R. V. Bellamkonda, "Controlled targeting of liposomal doxorubicin via the folate receptor in vitro," *Journal of Controlled Release*, vol. 92, no. 1-2, pp. 49–67, 2003.

[27] E. K. Rowinsky and R. C. Donehower, "Paclitaxel (taxol)," *The New England Journal of Medicine*, vol. 332, no. 15, pp. 1004–1014, 1995.

[28] T. K. Jain, J. Richey, M. Strand, D. L. Leslie-Pelecky, C. A. Flask, and V. Labhasetwar, "Magnetic nanoparticles with dual functional properties: drug delivery and magnetic resonance imaging," *Biomaterials*, vol. 29, no. 29, pp. 4012–4021, 2008.

[29] L. Shan, S. Cui, C. Du et al., "A paclitaxel-conjugated adenovirus vector for targeted drug delivery for tumor therapy," *Biomaterials*, vol. 33, no. 1, pp. 146–162, 2012.

[30] T. López, S. Recillas, P. Guevara, J. Sotelo, M. Alvarez, and J. A. Odriozola, "Pt/TiO_2 brain biocompatible nanoparticles: GBM treatment using the C6 model in Wistar rats," *Acta Biomaterialia*, vol. 4, no. 6, pp. 2037–2044, 2008.

[31] J. W. Seo, J. Ang, L. M. Mahakian et al., "Self-assembled 20-nm ^{64}Cu-micelles enhance accumulation in rat glioblastoma," *Journal of Controlled Release*, vol. 220, pp. 51–60, 2015.

[32] S. Stojković, A. Podolski-Renić, J. Dinić et al., "Development of resistance to antiglioma agents in rat C6 cells caused collateral sensitivity to doxorubicin," *Experimental Cell Research*, vol. 335, no. 2, pp. 248–257, 2015.

[33] Y.-G. Han, J. Xu, Z.-G. Li, G.-G. Ren, and Z. Yang, "In vitro toxicity of multi-walled carbon nanotubes in C6 rat glioma cells," *NeuroToxicology*, vol. 33, no. 5, pp. 1128–1134, 2012.

[34] B. Tang, G. Fang, Y. Gao et al., "Lipid-albumin nanoassemblies co-loaded with borneol and paclitaxel for intracellular drug delivery to C6 glioma cells with P-gp inhibition and its tumor targeting," *Asian Journal of Pharmaceutical Sciences*, vol. 10, no. 5, pp. 363–371, 2015.

[35] T. Tagami, Y. Imao, S. Ito, A. Nakada, and T. Ozeki, "Simple and effective preparation of nano-pulverized curcumin by femtosecond laser ablation and the cytotoxic effect on C6 rat glioma cells in vitro," *International Journal of Pharmaceutics*, vol. 468, no. 1-2, pp. 91–96, 2014.

[36] J.-L. Bridot, A.-C. Faure, S. Laurent et al., "Hybrid gadolinium oxide nanoparticles: multimodal contrast agents for in vivo imaging," *Journal of the American Chemical Society*, vol. 129, no. 16, pp. 5076–5084, 2007.

[37] A. T. M. Anishur Rahman, P. Majewski, and K. Vasilev, "Gd_2O_3 nanoparticles: Size-dependent nuclear magnetic resonance," *Contrast Media and Molecular Imaging*, vol. 8, no. 1, pp. 92–95, 2013.

[38] T. S. Renuga Devi and S. Gayathri, "FTIR And FT-Raman spectral analysis of Paclitaxel drugs," *International Journal of Pharmaceutical Sciences Review and Research*, vol. 2, no. 2, pp. 106–110, 2010.

[39] J. Zhang, S. Rana, R. S. Srivastava, and R. D. K. Misra, "On the chemical synthesis and drug delivery response of folate receptor-activated, polyethylene glycol-functionalized magnetite nanoparticles," *Acta Biomaterialia*, vol. 4, no. 1, pp. 40–48, 2008.

[40] Q. Yuan, S. Hein, and R. D. K. Misra, "New generation of chitosan-encapsulated ZnO quantum dots loaded with drug: synthesis, characterization and in vitro drug delivery response," *Acta Biomaterialia*, vol. 6, no. 7, pp. 2732–2739, 2010.

[41] D. Bhattacharya, M. Das, D. Mishra et al., "Folate receptor targeted, carboxymethyl chitosan functionalized iron oxide nanoparticles: a novel ultradispersed nanoconjugates for bimodal imaging," *Nanoscale*, vol. 3, no. 4, pp. 1653–1662, 2011.

[42] R. W. Brown, Y.-C. Norman Cheng, E. Mark Haacke, M. R. Thompson, and R. Venkatesan, *Magnetic Resonance Imaging: Physical Principles and Sequence Design*, John Wiley & Sons, 2014.